CHAPTER

4

BACKSCATTERING

SPECTROMETRY

J. A. Leavitt and L. C. McIntyre, Jr.

University of Arizona, Tucson, Arizona

M. R. Weller

Middle Tennessee State University, Murfreesboro, Tennessee

CONTENTS

4.1 INTRODUCTION

Backscattering spectrometry using ion beams with energies in the MeV range has been used extensively for accurate determination of stoichiometry, elemental areal density, and impurity distributions in thin films. Measurement of the number and energy distribution of ions backscattered from atoms in the near-surface region of solid materials allows identification of the atomic masses and determination of the distribution of target elements as a function of depth below the surface.

Application of the technique to thin film analysis is illustrated in Fig. 4.1 for the ideal case of a two-element thin film of uniform composition on a low-mass substrate. Analysis ions scatter elastically from target atoms with energy characteristic of the mass of the struck particle; they also lose energy passing into and out of the film material. Energy analysis of the backscattered ions by the detection system yields the backscattering spectrum displayed in the lower portion of Fig. 4.1 in the form of counts per channel vs. channel number. The channel number is normally linearly related to the backscattered ion energy, E_1. Appearing in the spectrum is a nearly flat-topped "peak" for each element present in the film. The peak widths are caused by the energy loss of the analysis ions in the film material.

The film elements may be identified by insertion of measured energies (E_1^A, E_1^B) of the high-energy sides of the peaks into

$$K_i \equiv E_1^i / E_0 \qquad (4.1)$$

to calculate the kinematic factor K for the ith element. E_0 is the incident ion laboratory kinetic energy. In turn, the kinematic factor, K, is given by

$$K = \left[\frac{\left(M_2^2 - M_1^2 \sin^2 \theta\right)^{1/2} + M_1 \cos \theta}{M_1 + M_2} \right]^2 \qquad (4.2)$$

where θ is the laboratory angle through which the incident ion is scattered, and M_1 and M_2 are the masses of the incident and target particles, respectively. Since the parameters M_1, E_0, and θ are usually known, M_2 is determined and the target element is identified.

The areal density, $(Nt)_i$, in atoms per unit area, may be determined for the ith element from knowledge of the
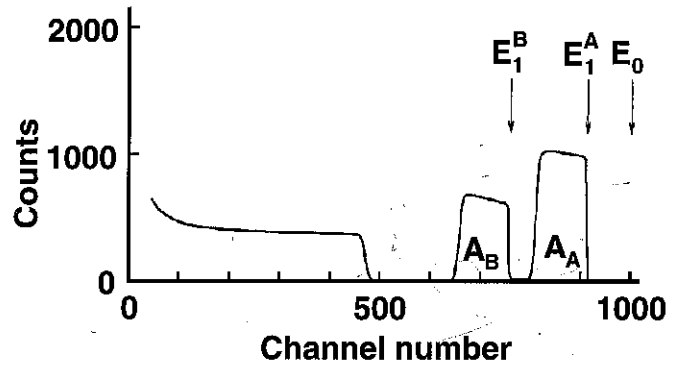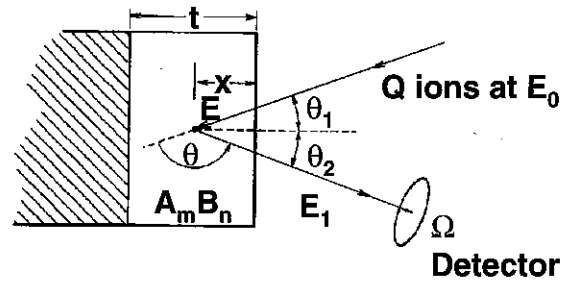
FIG. 4.1. Basic backscattering spectrometry. Experimental geometry (upper figure). Backscattering spectrum (lower figure) for the two-element compound ($A_m B_n$) film of uniform composition on a low-mass substrate.

detector solid angle, Ω, the integrated peak count A_i for Q incident ions, and the measured or calculated cross section $\sigma_i(E,\theta)$ using

$$(Nt)_i = \frac{A_i \cos \theta_1}{Q \Omega \sigma_i (E, \theta)} \qquad (4.3)$$

Here, N_i is the atomic density (atoms per unit volume) of the ith element and t is the physical film thickness. If the scattering is Rutherford (pure Coulomb scattering), then $\sigma_i(E,\theta)$ may be calculated from

$$\sigma_R (E, \theta) = \left(\frac{Z_1 Z_2 e^2}{4E} \right)^2$$

$$\times \frac{4 \left[\left(M_2^2 - M_1^2 \sin^2 \theta\right)^{1/2} + M_2 \cos \theta \right]^2}{M_2 \sin^4 \theta \left(M_2^2 - M_1^2 \sin^2 \theta\right)^{1/2}} \qquad (4.4)$$

where Z_1 and Z_2 are the atomic numbers of the incident and target ions, respectively. This equation is given in cgs units. A useful number in evaluating this equation is $e^2 \simeq 1.44 \times 10^{-13}$ MeV cm. For very thin films, E, the analysis ion energy immediately before scattering, may be taken as E_0. For thicker films, the mean energy of the analysis ions in the film should be used for E (see 4.2.4.6).

The average stoichiometric ratio for the compound film ($A_m B_n$) may be calculated from Eq. (4.3) to be

$$\frac{n}{m} = \frac{N_B}{N_A} = \frac{A_B}{A_A} \cdot \frac{\sigma_A(E, \theta)}{\sigma_B(E, \theta)} \quad . \qquad (4.5)$$

Note that this ratio depends only on the ratio of measured integrated peak counts A_A/A_B and knowledge of the cross section ratio σ_A/σ_B. The hard-to-measure quantities Q and Ω have cancelled.

Conversion of areal densities, $(Nt)_i$, to physical film thickness, t, requires knowledge of the film density, ρ_{AB}. The relevant atomic densities, N_A^{AB} and N_B^{AB}, may be calculated from

$$N_A^{AB} = \frac{m \rho_{AB} N_0}{M_{AB}} \quad ; \quad N_B^{AB} = \frac{n \rho_{AB} N_0}{M_{AB}} \qquad (4.6)$$

and then used in

$$t = \frac{(Nt)_A}{N_A^{AB}} = \frac{(Nt)_B}{N_B^{AB}} \qquad (4.7)$$

to calculate t. Here, N_0 is Avogadro's number and $M_{AB} = m M_A + n M_B$ is the molecular weight of compound $A_m B_n$.

Typical uncertainties in the results are $\pm 3\%$ for areal densities and a few tenths of 1% for average stoichiometric ratios. The actual uncertainty in the physical film thickness is usually unknown since the film densities are usually unknown.

The preceding discussion indicates the power of backscattering spectrometry for analysis of a simple film (see 4.3.1.1 for further experimental details). Historically, the majority of backscattering analyses have been performed using ^{4}He analysis ions with energies in the 1-2 MeV region. The reasons for this are: (1) the available accelerators produced beams with these energies, (2) data for the energy loss of ^{4}He in the elements were better known than for other ions, (3) silicon surface barrier detector energy resolution for ^{4}He is about 15 keV, and most importantly, (4) the backscattering cross sections for ^{4}He

incident on all elements more massive than Be are nearly Rutherford in this energy region.

The principal strengths of Rutherford backscattering (RBS) with ^{4}He ions are: (1) it is an absolute method that does not require the use of standards; meaningful uncertainties can usually be assigned to the results; (2) it is quick and easy; typical data acquisition time is about ten minutes; (3) it is frequently non-destructive, and (4) it may be used for depth profiling (with 10-30 nm depth resolution). The technique's principal weakness is that it is not good for trace-element analysis. It has moderate sensitivity ($\sim 10^{-4}$) to heavy elements in or on light matrices but very poor sensitivity ($\sim 10^{-1}$) to light elements in or on heavy matrices.

Recent years have seen increasing use of higher-energy light ions (^{1}H,^{4}He), higher-energy heavy ions (^{16}O,^{35}Cl), and even lower-energy ions (^{4}He,^{12}C) for backscattering analyses. The higher-energy light ions are used to improve the accuracy of measured stoichiometric ratios by reducing backscattering peak overlap, and to improve mass resolution and sensitivity to light elements. The cross sections are non-Rutherford for light target elements. The higher-energy heavy ions are used to improve mass and depth resolution and enhance the sensitivity to medium and heavy elements. The lower-energy ions are used to improve mass and depth resolution and sensitivity for all elements. Recent detector developments, particularly for time-of-flight and electrostatic analyzers, have made the use of the lower-energy ions feasible.

It is the aim of this chapter to present basic equations and tabular and graphical data needed to analyze backscattering spectra. A few examples illustrating how this information is used for the analyses are included. For a more extensive discussion of the principles of backscattering spectrometry, see Chu et al. (1978). Although this chapter is not a review of recent advances in the field, it concludes with a succinct discussion of experimental considerations that may be of use to the analyst in choosing the experimental set-up that will produce optimum data.

4.2 FUNDAMENTALS

4.2.1 The kinematic factor and mass resolution

Equation (4.2), the expression for the kinematic factor K, results from application of conservation of energy and

momentum to the two-body collision between isolated particles of masses M_1 and M_2. Incident beam particle 1 (at laboratory kinetic energy E_0) is scattered with final laboratory kinetic energy E_1 through laboratory angle θ by target particle 2 (initially at rest in the laboratory). The binding energy of particle 2 in the target is neglected. The kinematic factor is independent of the nature of the force between the particles (as long as energy is conserved). Tables of kinematic factors, K, are included in Appendix 5 for scattering of ^1H and ^4He. The kinematic factors for other ions can be calculated by using Eq. (4.2). Average kinematic factors, $\overline{K}$, are also listed. The average mass $\overline{M_2}$, for natural isotopic abundance, has been used in the calculation of $\overline{K}$ [Eq. (4.2)].

For fixed θ, the energy separation, ΔE_1, for beam particles scattered by target particles of mass difference ΔM_2 is [from Eq. (4.1)]:

$$\Delta E_1 = E_0 \left(\frac{dK}{dM_2} \right) \Delta M_2 \quad . \tag{4.8}$$

If ΔE_1 is set equal to δE, the minimum energy separation that can be experimentally resolved, then δM_2, the mass resolution of the system is

$$\delta M_2 = \frac{\delta E}{E_0 \left(\dfrac{dK}{dM_2} \right)} \quad . \tag{4.9}$$

Figure 4.2 contains information that may be used to estimate δM_2 for a given experimental situation if the overall energy resolution, δE, is known. The quantity δE contains contributions from detector resolution, straggling, beam energy spread, and various geometric effects (O'Connor and Chunyu, 1989).

The mass resolution at the sample surface is usually determined primarily by the detector resolution; straggling dominates for layers deep in the sample. For fixed $\delta E/E_0$, Fig. 4.2 indicates that δM_2 improves with increasing analysis beam mass. This is somewhat deceptive since δE frequently depends on the analysis beam mass. For instance, if a typical surface barrier detector is used with 5 MeV ^4He and ^{12}C analysis beams, then δM_2 at $M_2 = 100$ u is actually somewhat better (2.2 u vs. 3.2 u) for ^4He than for ^{12}C because the detector resolution is ~15 keV for ^4He and ~50 keV for ^{12}C at 5 MeV (Leavitt et al., 1988). There are, of course, instances where the detector resolution improves with increase in beam mass; such is the case for the time-of-flight detector.
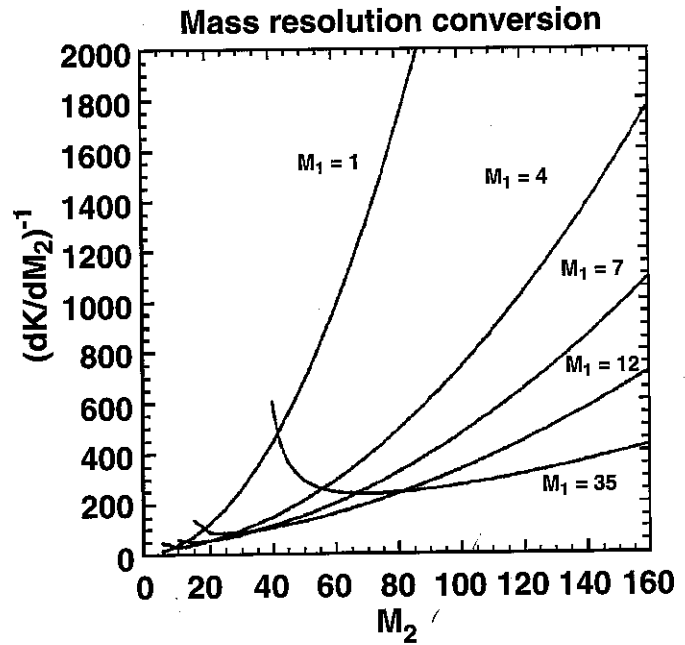

Mass resolution conversion

FIG. 4.2. Plots of $(dK/dM_2)^{-1}$ vs. target mass M_2 for several analysis beams (M_1 = ion mass). Units of M_1 and M_2 are u. The laboratory backscattering angle is 180°. The plots may be used to estimate the mass resolution $\delta M_2 = (\delta E/E_0) (dK/dM_2)^{-1}$ if $\delta E/E_0$ is specified.

4.2.2 Elastic scattering cross sections

4.2.2.1 Definition of the differential cross section

The average differential cross section, $\sigma(\theta, E)$, for scattering of beam particles of incident energy E by target particles in a thin film is defined by

$$\sigma(\theta, E) \equiv \left(\frac{1}{Nt} \right) \frac{dQ(E)}{Q} \frac{1}{\Omega(\theta)} \tag{4.10}$$

where Nt is the number of target atoms/unit area perpendicular to the beam, and $[dQ(E)]/Q$ is the fraction of incident particles scattered into the small solid angle $\Omega(\theta)$ centered at deflection angle θ. If $dQ(E)$ is replaced by A and subscripts i added, Eq. (4.3) results.

4.2.2.2 Rutherford cross sections

If the force between the incident nucleus $(M_1, Z_1 e, E)$ and the target nucleus $(M_2, Z_2 e$, initially at rest) is assumed to be the Coulomb force, $\vec{F}_{12} = (Z_1 Z_2 e^2 / r^2) \hat{r}$, then use of the above definition results in Eq. (4.4), the expression for the Rutherford cross section in the

41

laboratory system. Numerical values of laboratory Rutherford cross sections for beams of ^{1}H, ^{4}He, ^{7}Li, ^{12}C, and ^{14}Si at 1 MeV incident energies are given in Appendix 6 for several backscattering angles. An accurate approximation for large backscattering angles and $(M_1/M_2) \ll 1$ is Chu *et al.* (1978)

$$\sigma_R(E,\theta) \simeq 0.02073 \left(\frac{Z_1 Z_2}{4E}\right)^2 \left[\sin^{-4}\left(\frac{\theta}{2}\right) - 2\left(\frac{M_1}{M_2}\right)^2\right] \quad (4.11)$$

with E in MeV and σ_R in b/sr [1b (barn) = 10^{-24} cm^2].

4.2.2.3 Non-Rutherford cross sections

Experimental measurements indicate that actual cross sections depart from Rutherford at both high and low energies for all projectile-target pairs. The low-energy departures are caused by partial screening of the nuclear charges by the electron shells surrounding both nuclei. Results of several investigations (L'Ecuyer *et al.*, 1979; Hautala and Luomajärvi, 1980; Andersen *et al.*, 1980; MacDonald *et al.*, 1983; and Wenzel and Whaling, 1952) indicate that these low-energy corrections are given with adequate accuracy by L'Ecuyer *et al.* (1979)

$$\sigma/\sigma_R = 1 - \frac{0.049\, Z_1 Z_2^{4/3}}{E_{CM}} \quad (4.12)$$

or by (Wenzel and Whaling, 1952)

$$\sigma/\sigma_R = 1 - \frac{0.0326\, Z_1 Z_2^{7/2}}{E_{CM}} \quad (4.13)$$

for light-ion analysis beams with MeV energies. Here E_{CM} is the center-of-mass kinetic energy in keV. In practice, replacing E_{CM} by E_{Lab} produces negligible error. A table of low-energy corrections is given in Appendix 6. Algorithms for rapid computations of cross sections for medium energy (50 - 1000 keV) backscattering are discussed by Mendenhall and Weller (1991a).

The high-energy departures of the cross sections from Rutherford behavior are caused by the presence of short-range nuclear forces. Recent measurements and calculations (Bozoian *et al.*, 1990; Bozoian, 1991a and 1991b; and Hubbard *et al.*, 1991) regarding the onset of these high-energy departures are summarized in Fig. 4.3 for ^{1}H, ^{4}He, and ^{7}Li analysis beams. The straight lines on Fig. 4.3 represent rough boundaries separating the region of Rutherford behavior (below the line) from the region of
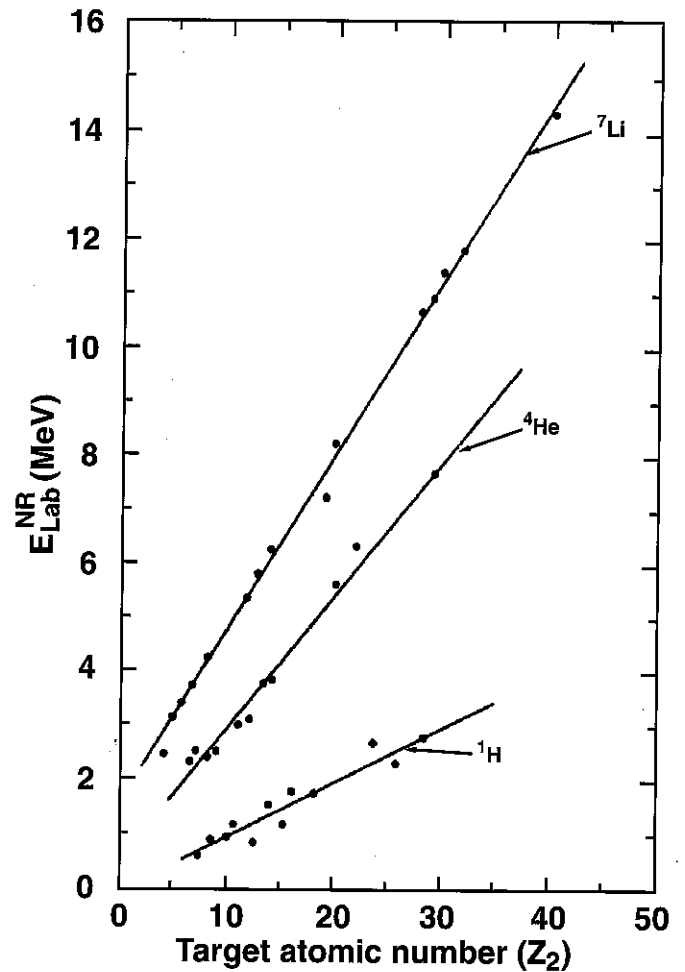
FIG. 4.3. Laboratory projectile energies, E_{Lab}^{NR}, at which backscattering cross sections (for $160° < \Theta_{Lab} < 180°$) deviate from Rutherford by 4% vs. target atomic number Z_2, for ^{1}H, ^{4}He, and ^{7}Li projectiles. The straight lines are least squares fitted to the data points [Eq. (4.14)]. The ^{1}H and ^{4}He points are experimental (see Bozoian, 1991b for references). The ^{7}Li data were obtained from optical model calculations (Bozoian, 1991a).

non-Rutherford behavior (above the line). Equations resulting from the least-squares fits to the points in Fig. 4.3 are

For ^{1}H: $E_{Lab}^{NR} \simeq (0.12 \pm 0.01)\, Z_2 - (0.5 \pm 0.1)$

For ^{4}He: $E_{Lab}^{NR} \simeq (0.25 \pm 0.01)\, Z_2 + (0.4 \pm 0.2)$ (4.14)

For ^{7}Li: $E_{Lab}^{NR} \simeq (0.330 \pm 0.005)\, Z_2 + (1.4 \pm 0.1)$

where E_{Lab}^{NR} is the laboratory projectile kinetic energy (in MeV) at which the backscattering cross section (for $160° < \theta_{Lab} < 180°$) deviates from Rutherford by 4% for a target atom of atomic number Z_2. Note that cross sections for backscattering of ^{1}H at 1 MeV are non-Rutherford for $Z_2 \lesssim 15$, while cross sections for ^{4}He at 2 MeV are Rutherford for $Z_2 \gtrsim 6$. At present, no practical method exists for rapid accurate calculation of these high-energy non-Rutherford cross sections; they must be measured.

Advantages associated with the use of non-Rutherford cross sections such as improved accuracy in determination of stoichiometric ratios and increased sensitivity for detection of light elements in heavy-element matrices frequently justify the additional work required to make the measurements. According to Eq. (4.5), the average stoichiometric ratio for two film elements depends only on the ratio of integrated peak counts, A_A/A_B, and the cross section ratio, σ_B/σ_A. These stoichiometric ratios may be determined as accurately as a few tenths of a percent by acquisition of sufficient data if the backscattering peaks are well separated and if the cross section ratios are accurately known. However, use of analysis ion energies such that the cross sections are Rutherford (and therefore accurately known) frequently produces backscattering peaks that overlap. The uncertainties in the peak count ratios resulting from deconvolution/simulation techniques often severely limit the accuracies of the stoichiometric ratios, particularly in cases of non-uniform film composition.

Use of higher analysis ion energies usually results in desired reduction of peak overlap since the energy loss of the analysis ions in matter decreases with increasing energy in the energy range normally used. However, the accuracy of the cross section ratio may be adversely affected if the cross sections of interest are non-Rutherford at the higher ion energy. The analysis ion energy should usually be chosen to be as high as possible to take advantage of the reduction in peak overlap, but with a value such that the relevant cross sections have accurately measured values that do not vary wildly in the region just below the incident ion energy. If the ratio of measured-to-Rutherford cross section varies slowly with energy, the non-Rutherford effect may be easily included in calculations using Eqs. (4.3) and (4.5) by simply dividing the A_i by the non-Rutherford enhancement factors $(\sigma/\sigma_R)_i$ at the mean energy of the projectile in the film and proceeding with the calculation as if the cross sections were Rutherford. Since non-Rutherford cross sec-

tions for light target elements are frequently many times Rutherford, while corresponding cross sections for the heavier target elements may remain Rutherford, increased relative sensitivity for light element detection results. For example, the relative sensitivity for detection of C in thin films on Si substrates is enhanced relative to Rutherford by a factor of 7 for 3.8 MeV ^{4}He and by a factor of more than 100 for 4.27 MeV ^{4}He. In another instance, ^{4}He ions with energies 8.1–9.1 MeV have recently been used to enhance the sensitivity for detection of O in superconducting films by a factor of ~25 over Rutherford (Martin et al., 1988; Barbour et al., 1988).

Strong, narrow, isolated resonances in the non-Rutherford cross sections may be used for depth profiling light elements in or on heavy matrices. Examples are the 3.04 MeV resonance in the ^{4}He-^{16}O cross section (Cameron, 1953), the 2.525 MeV resonance in the ^{1}H-^{9}Be cross section (Mozer, 1956; Leavitt et al., 1994), and the 4.26 MeV resonance in the ^{4}He-^{12}C cross section (Bittner and Moffat, 1954).

There is considerable information in the literature regarding measured non-Rutherford cross sections for ^{1}H and ^{4}He projectiles. Most of these data were acquired during the 1950s and 1960s in connection with nuclear level structure studies. The data have usually been presented in graphical form only, as differential cross sections in the center-of-mass system vs. projectile energy in the laboratory system. An unpublished compilation (Jarjis, 1979) gives some tables of numerical values produced by use of a computer digitizer. A few more recent reports contain tabular as well as graphical data on the measured cross sections. Non-Rutherford cross section information for ^{1}H and ^{4}He analysis beams is presented in Appendix 7.

4.2.3 Experimental geometry

Two experimental arrangements in common use are referred to as the IBM and Cornell geometries. For both geometries, the incident beam is horizontal and the sample surface vertical. For the IBM geometry, the scattered beam (directed at the detector), the incident beam, and the sample normal are all in the same horizontal plane. In the Cornell geometry the detector is directly below the incident beam; the incident beam and the scattered beam are in a vertical plane. In both geometries the angle between the sample normal and the incident beam is θ_1 and the angle between the sample normal and

the scattered beam is θ_2. The "tilt" axis is a vertical axis through the beam spot on the sample surface, so the "tilt" angle is θ_1 (see Fig. 4.1) in both cases. The relation between the scattering angle θ and θ_1 and θ_2 is $\theta = \pi - |\theta_1 \pm \theta_2|$ for the IBM geometry and $\cos\theta_2 = \cos(\pi - \theta)\cos\theta_1$ for the Cornell geometry. In the IBM geometry, for a given tilt angle θ_1, the angle θ_2 depends on the direction of θ_1, i.e., whether the sample normal is rotated toward or away from the direction of the scattered beam. The relation between the inward and outward path lengths and the perpendicular distance x below the sample surface at which a backscattering event took place is given by

$$d_{in} = \frac{x}{\cos\theta_1} \; ; \; d_{out} = \frac{x}{\cos\theta_2} \quad \text{(IBM)}$$

$$d_{in} = \frac{x}{\cos\theta_1} \; ; \; d_{out} = \frac{x}{\cos\theta_1 , \cos\theta_2} \quad \text{(Cornell)} \quad (4.15)$$

4.2.4 Effects of energy loss of ions in solids

4.2.4.1 Definitions

Many of the features of a backscattering spectrum are determined by the energy loss of the analysis beam ions as they traverse the sample material. Consequently, a quantitative knowledge of this energy loss is a key element in understanding a backscattering spectrum. This section offers only a brief summary of the relevant quantities and relations relating to energy loss, but a full exposition is given in Chapter 2.

The stopping power of a material for a particular ion is usually defined as the energy loss per distance travelled in the material, denoted as dE/dx. This quantity depends on the ion and the material traversed as well as the energy of the ion. Usual units of the stopping power are $eV/\text{Å}$ or eV/nm.

Another quantity, the stopping cross section ε, is defined as the energy loss/atom/cm^2 (areal density) of material traversed. This quantity is independent of the volume density of the material. Usual units are 10^{-15} eV cm^2. The relation between these two quantities is given by

$$\frac{dE}{dx} = N\varepsilon \quad (4.16)$$

where N is the atomic density (atoms/cm^3). The reader should be aware that the literature is not consistent in these definitions, and a common unit of "stopping power" used in nuclear physics is $eV/(mg/cm^2)$ where the material "thickness" is given in units of mg/cm^2 (actually an areal density) (Northcliffe and Schilling, 1970).

Values of ion stopping cross sections in all elements are available from an extensive study based on semi-empirical fitting of experimental data (Ziegler *et al.*, 1985). A parameterization of proton stopping cross sections involving eight parameters per element is given together with scaling rules for extension to any analysis ion (see Appendix 3, Section 3.2). The variation of stopping cross section for ^{4}He ions with energy is similar for all elements, showing a broad maximum below about 1 MeV. The decrease in energy loss of ^{4}He ions with increasing energy above about 1 MeV is responsible for the fact that the elemental peak widths in a backscattering spectrum are narrower at higher incident energies in this energy range.

An approximation, the Bragg rule (Bragg and Kleeman, 1905), is commonly used to calculate stopping cross sections of ions in compounds or mixtures of different elements. This approximation simply assumes that each target atom acts independently in the energy loss process and ignores any effects of chemical bonding in the material. This rule can be expressed for a compound A_mB_n by

$$\varepsilon^{A_mB_n} = m\varepsilon^A + n\varepsilon^B \quad (4.17)$$

which gives the compound stopping cross section in terms of energy loss/molecule/cm^2 traversed. The corresponding stopping power is given by

$$\left(\frac{dE}{dx}\right)^{AB} = N^{AB}\varepsilon^{AB} = N_A^{AB}\varepsilon^A + N_B^{AB}\varepsilon^B \quad (4.18)$$

where N^{AB} is the molecular density (molecules/cm^3) and N_A^{AB} and N_B^{AB} are the atomic densities of A and B in the compound (the m and n subscripts on A and B are suppressed in this notation). (See Example 4.1.) Deviations from the Bragg rule have been reported and a discussion of the effect of chemical binding on stopping powers is given in Ziegler and Manoyan (1988) (also see 2.2.3.4.).

EXAMPLE 4.1. Calculate the stopping cross section and stopping power of 2 MeV ^{4}He$^+$ in Al$_2$O$_3$ using the Bragg rule. Use tabulated values of stopping cross sections (see Appendix 3, Section 3.1), $\varepsilon^{Al} = 44 \times 10^{-15}$ eV cm^2 and $\varepsilon^O = 35 \times 10^{-15}$ eV cm^2 in Eq. (4.17) to find

$$\varepsilon^{Al_2O_3} = (2 \times 44 + 3 \times 35) \times 10^{-15}$$

$$= 193 \times 10^{-15} \text{ eV cm}^2 \ .$$

To find $(dE/dx)^{Al_2O_3}$ we calculate the molecular density $N^{Al_2O_3}$ as

$$N^{Al_2O_3} = \frac{\rho N_0}{M} = \frac{4 \frac{gm}{cm^3} \times 6 \times 10^{23} \frac{molecules}{mole}}{102 \frac{gm}{mole}}$$

$$= 2.35 \times 10^{22} \frac{Al_2O_3}{cm^3} \ .$$

The stopping power is obtained from Eq. (4.18)

$$\left(\frac{dE}{dx}\right)^{Al_2O_3} = N^{Al_2O_3} \ \varepsilon^{Al_2O_3}$$

$$= 2.35 \times 10^{22} \times 193 \times 10^{-15}$$

$$= 46 \frac{eV}{\text{Å}} \ .$$

An alternate method, using an atomic basis, involves calculating the atomic densities of each element in the molecule.

$$N_{Al}^{Al_2O_3} = 2 \times 2.35 \times 10^{22} = 4.7 \times 10^{22} \text{ Al/cm}^3$$

and

$$N_O^{Al_2O_3} = 3 \times 2.35 \times 10^{22} = 7.1 \times 10^{22} \text{ O/cm}^3 \ .$$

Using the second equality in Eq. (4.18), we find:

$$\left(\frac{dE}{dx}\right)^{Al_2O_3} = N_{Al}^{Al_2O_3} \ \varepsilon^{Al} + N_O^{Al_2O_3} \ \varepsilon^O$$

$$= 4.7 \times 10^{22} \times 44 \times 10^{-15}$$

$$+ 7.1 \times 10^{22} \times 35 \times 10^{-15}$$

$$= 46 \times 10^8 \frac{eV}{cm}$$

$$= 46 \frac{eV}{\text{Å}}$$

The calculation of energy loss, ΔE, of ions traversing a solid involves the integration of the stopping power as in

$$\Delta E = \int \frac{dE}{dx} dx \ . \tag{4.19}$$

In cases of thin targets the stopping power can often be taken as constant, evaluating the necessary quantities at the incident energy (surface energy approximation) or at the mean energy of the beam in the target (mean energy approximation). In the case of thick targets, a computer is usually used to calculate the energy of ions at a depth below the sample surface by numerical integration of Eq. (4.19), dividing the target material into thin slabs and using a parameterization to calculate the stopping power at successive ion energies. Notice that calculation of ion energy loss requires a knowledge of the composition of the sample, which may be the object of the analysis and therefore unknown. An iterative procedure is often required in such cases, initially using an assumed composition to calculate an initial approximation of energy loss which is in turn used in calculating improved values of the composition (see 4.3.1.1).

The range of ion beams in materials and the phenomena of energy straggling are also of importance in understanding a backscattering spectrum (see Chapter 2). Range

information can be used to estimate the maximum analysis depth possible with a given beam at a given incident energy. Recall, however, that the beam must scatter and reemerge from the sample to be useful in backscattering analysis. A rough criteria for accessible depth proposed by Chu *et al.* (1978) is that the energy of the scattered particle at the detector should be greater than 1/4 the incident energy.

4.2.4.2 Depth scale

To utilize the depth profiling capabilities of backscattering it is necessary to relate the energy of the scattered particle to the depth in the sample where the scattering occurred. This depends on the energy loss of the analysis ion traversing the sample, the kinematic factor for the scattering, and the orientation of the sample normal relative to both the incident beam and the detector direction. We denote the difference in energy at the detector of a particle scattered at the surface and a particle scattered at a depth x, measured perpendicular to the sample surface, as ΔE. This quantity is given as a function of x by

$$\Delta E = [S] \, x \qquad (4.20)$$

where [S] is called the energy loss factor and is defined by

$$[S] = \left[K \left(\frac{dE}{dx} \right)_{in} \frac{1}{\cos \theta_1} + \left(\frac{dE}{dx} \right)_{out} \frac{1}{\cos \theta_2} \right] . \qquad (4.21)$$

The kinematic factor K and the angles θ_1 and θ_2 are defined in Sections 4.2.1 and 4.2.3, and the stopping powers are those for the analysis ion on the inward and outward path.

The corresponding relation involving the areal density and stopping cross sections is given by

$$\Delta E = [\varepsilon] \, Nx \qquad (4.22)$$

for a single element sample. The quantity [ε] is called the stopping cross section factor and is defined by

$$[\varepsilon] = \left[K \, \varepsilon_{in} \frac{1}{\cos \theta_1} + \varepsilon_{out} \frac{1}{\cos \theta_2} \right] . \qquad (4.23)$$

For multi-element samples, we see that the depth-energy relation depends on the struck particle; therefore, separate relations must be calculated for each element in the sample. In the case of a compound $A_m B_n$, N becomes the molecular density (molecules/cm^3) N^{AB} and corresponding values of K and ε_{out} which apply for scattering from

elements A or B are used in the stopping cross section factor. The relations for element *A* are given in Eqs. (4.24) and (4.25).

$$\Delta E_A = [\varepsilon]_A^{AB} \, N^{AB} \, x \qquad (4.24)$$

$$[\varepsilon]_A^{AB} = \left[K_A \, \varepsilon_{in}^{AB} \frac{1}{\cos \theta_1} + \varepsilon_{out, A}^{AB} \frac{1}{\cos \theta_2} \right] . \qquad (4.25)$$

Similar relations can be written for element B. The lower index refers to the scattering element and the upper index refers to the stopping material. A surface energy approximation is often used for stopping cross section factors. In this appoximation, ε_{in} is evaluated at the incident energy E_0 and ε_{out} is evaluated at energy KE_0. The resulting stopping cross section factor is usually written [ε_0]. (See Example 4.2.)

Since both the energy loss factor and stopping cross section factor require evaluation of energy dependent parameters, an integral over the relevant energies should be performed. In many cases use of the incident beam energy (surface—energy approximation) or the mean beam energy in the sample (mean—energy approximation) is satisfactory.

4.2.4.3 Depth resolution

The considerations in the previous section lead to an expression for the depth resolution in backscattering analysis. Using Eq. (4.20) we see that the minimum detectable depth difference, δx, is related to the minimum detectable scattered particle energy difference, δE, by

$$\delta x = \frac{\delta E}{[S]} . \qquad (4.26)$$

Sources of energy spread include detector resolution, energy spread in the incident beam, straggling, and kinematic effects. Since energy straggling increases as the ion beam traverses the sample, the depth resolution degrades with depth in the sample. A common practice is to quote depth resolution at the surface which need not include a straggling contribution. A convenient approximation is to assume all sources of energy spread are Gaussian and to add them in quadrature.

The depth resolution can be improved by increasing [S]. This is usually done by tilting the sample normal relative to the incoming beam (i.e., increasing θ_1 and/or

EXAMPLE 4.2. Calculate the depth-scattered ion energy differences for 2 MeV $^4\text{He}^+$ in Al_2O_3. We again consider the case $\theta_1 = 0$ and $\theta_2 = 10°$. Here we must calculate separate differences for Al and O. The Al and O stopping cross section factors are calculated using Eq.(4.25). The K factors for ^4He on Al and O are 0.5525 and 0.3625, respectively, resulting in energies after scattering (at the surface) of $0.5525 \times 2.0 = 1.105$ MeV for Al and $0.3625 \times 2.0 = 0.725$ MeV for O. We evaluate the elemental stopping cross sections involved in $\varepsilon_{out,Al}^{Al_2O_3}$ and $\varepsilon_{out,O}^{Al_2O_3}$ at these energies using the surface energy approximation.

$$\varepsilon_{in}^{Al_2O_3} = 2 \times \varepsilon_{in}^{Al} + 3 \times \varepsilon_{in}^{O} = 2 \times 44 \times 10^{-15}$$
$$+ 3 \times 35 \times 10^{-15} = 193 \times 10^{-15} \text{ eV cm}^2$$

$$\varepsilon_{out,Al}^{Al_2O_3} = 2 \times \varepsilon_{out,Al}^{Al} + 3 \times \varepsilon_{out,Al}^{O} = 2 \times 51 \times 10^{-15}$$
$$+ 3 \times 46 \times 10^{-15} = 240 \times 10^{-15} \text{ eV cm}^2$$

$$\varepsilon_{out,O}^{Al_2O_3} = 2 \times \varepsilon_{out,O}^{Al} + 3 \times \varepsilon_{out,O}^{O} = 2 \times 54 \times 10^{-15}$$
$$+ 3 \times 48 \times 10^{-15} = 252 \times 10^{-15} \text{ eV cm}^2 \quad .$$

We can now calculate the stopping cross section factors

$$[\varepsilon_0]_{Al}^{Al_2O_3} = K_{Al} \, \varepsilon_{in}^{Al_2O_3} \frac{1}{\cos \theta_1} + \varepsilon_{out,Al}^{Al_2O_3} \frac{1}{\cos \theta_2}$$

$$[\varepsilon_0]_{Al}^{Al_2O_3} = 0.5525 \times 193 \times 10^{-15} + 240 \times 10^{-15}$$
$$\times 1.015 = 350 \times 10^{-15} \text{ eV cm}^2$$

and

$$[\varepsilon]_{O}^{Al_2O_3} = K_O \, \varepsilon_{in}^{Al_2O_3} \frac{1}{\cos \theta_1} + \varepsilon_{out,O}^{Al_2O_3} \frac{1}{\cos \theta_2}$$

$$[\varepsilon_0]_{O}^{Al_2O_3} = 0.3625 \times 193 \times 10^{-15} + 252 \times 10^{-15}$$
$$\times 1.015 = 326 \times 10^{-15} \text{ eV cm}^2 \quad .$$

Using the molecular density $N^{Al_2O_3} = 2.35 \times 10^{22}$ molecules/cm^3, we find

$$\Delta E_{Al} = [\varepsilon_0]_{Al}^{Al_2O_3} \, N^{Al_2O_3} \, x = 82.3 \frac{\text{eV}}{\text{Å}} \times x$$

$$\Delta E_O = [\varepsilon_0]_{O}^{Al_2O_3} \, N^{Al_2O_3} \, x = 76.6 \frac{\text{eV}}{\text{Å}} \times x$$

where ΔE_{Al} and ΔE_O are the energies of ions scattered from Al and O relative to ions scattered at the surface and x is the depth in the target where the scattering took place.

θ_2). The effect is to increase the path length required to reach a given depth (measured perpendicular to the surface) in the sample. This increases the scattered particle energy difference for a given depth difference. It should be noted that the use of large tilt angles introduces additional sources of energy broadening and requires that the sample surface be reasonably flat. Several studies concerned with optimizing depth resolution by target tilting can be found in the literature (Williams and Moller, 1978; O'Conner and Chunyu, 1989; and Boerma et al., 1990).

4.2.4.4 Surface spectrum height

An important characteristic of a backscattering spectrum is the height (counts/channel) of the front edge of an elemental peak corresponding to scattering from the top surface of the sample. We consider here cases where the sample produces elemental peaks which are much wider than the energy resolution of the detection system. For a single-element target, the surface height is given by

$$H_0 = \sigma(E_0)\Omega Q \xi / ([\varepsilon_0] \cos \theta_1) \qquad (4.27)$$

where ξ is the energy width per channel and $[\varepsilon_0]$ is the surface energy approximation of the stopping cross section factor [defined in Eq. (4.23)] evaluated at the incident energy. The remaining symbols are those defined in Eq. (4.3). This equation is obtained from Eq. (4.3), where the areal density (Nt) contributing to one channel of the spectrum at the surface is $\xi/[\varepsilon_0]$ [see Eq. (4.22)].

The surface heights of the two elemental peaks in a compound $A_m B_n$ are given by

$$H_{A,0} = \sigma_A(E_0)\, \Omega Q m \mathcal{E}/([\varepsilon_0]_A^{AB} \cos \theta_1)$$

$$H_{B,0} = \sigma_B(E_0)\, \Omega Q n \mathcal{E}/([\varepsilon_0]_B^{AB} \cos \theta_1) \qquad (4.28)$$

where $[\varepsilon_0]_A^{AB}$ and $[\varepsilon_0]_B^{AB}$ are the compound stopping cross section factors as defined in Eq. (4.25) using the surface energy approximation.

The stoichiometry of a multi-element sample can be calculated by comparing surface heights of the elemental peaks (see 4.3.1.2 and Example 4.3).

4.2.4.5 Peak widths for thin films

The energy width of elemental peaks in single- or multi-elemental samples, where the peaks are at least partially resolved and wider than the system energy resolution, can be calculated from Eqs. (4.22) or (4.24) by replacing x by the film thickness t. Conversely, the elemental areal densities can be calculated from experimentally determined peak widths using these equations and a knowledge of stopping cross sections. This procedure is described in 4.3.1.3.

4.2.4.6 Mean energy in thin films

To calculate the mean energy of the analysis ions in a thin film containing r elements, use Eq. (4.3) with $E = E_0$ to calculate $(Nt)_i^{SEA}$ in the surface energy approximation (SEA). Calculate the energy loss of the ions passing through the film, ΔE_{in}^{SEA}, using

$$\Delta E_{in}^{SEA} = \sum_{i=1}^{r} \varepsilon^i (E_0)(Nt)_i^{SEA} \quad . \qquad (4.29)$$

Then calculate the mean energy of the ions in the film, $\overline{E}^{(1)}$, using

$$\overline{E}^{(1)} = E_0 - \frac{\Delta E_{in}^{SEA}}{2} \quad . \qquad (4.30)$$

This result represents a first order correction. The procedure should be iterated until $\overline{E}$ changes by less than a specified percentage between successive iterations. For the second iteration, the $(Nt)_i^{(1)}$ should be calculated using Eq. (4.3) with $E = \overline{E}^{(1)}$; then $\Delta E_{in}^{(1)}$ and $\overline{E}^{(2)}$ are calculated using

EXAMPLE 4.3. Calculate surface heights for 2 MeV ^{4}He$^+$ on Al_2O_3. We assume the following experimental parameters for this calculation:

$\Omega = 10^{-3}$ sr

$\mathcal{E} = 1$ keV/channel

$Q = 6.24 \times 10^{13}$ incident particles (10 μC charge)

$\theta_1 = 0, \theta_2 = 10°$ (scattering angle = 170°)

The Rutherford cross sections for Al and O are found in Appendix 6, to be 0.2128×10^{-24} cm^2/sr and 0.0741×10^{-24} cm^2/sr. The compound stopping cross section factors are those found in the depth scale Example 4.2:

$$[\varepsilon_0]_{Al}^{Al_2O_3} = 350 \times 10^{-15} \text{ eV cm}^2$$

$$[\varepsilon_0]_{O}^{Al_2O_3} = 326 \times 10^{-15} \text{ eV cm}^2 \quad .$$

Using Eq. (4.28), we find

$$H_{Al,0} = \frac{\sigma \Omega Q 2 \mathcal{E}}{[\varepsilon_0]_{Al}^{Al_2O_3}}$$

$$= \frac{0.2128 \times 10^{-24} \times 10^{-3} \times 6.24 \times 10^{13} \times 2 \times 10^3}{350 \times 10^{15}}$$

$$= 76 \text{ cts} \quad .$$

$$H_{O,0} = \frac{\sigma \Omega Q 3 \mathcal{E}}{[\varepsilon_0]_{O}^{Al_2O_3}}$$

$$= \frac{0.0741 \times 10^{-24} \times 10^{-3} \times 6.24 \times 10^{13} \times 3 \times 10^3}{326 \times 10^{15}}$$

$$= 43 \text{ cts (or particles / channel)} \quad .$$

$$\Delta E_{in}^{(1)} = \sum_{i=1}^{r} \varepsilon^i (\overline{E}^{(1)})(Nt)_i^{(1)} \qquad (4.31)$$

and

$$\overline{E}^{(2)} = E_0 - \frac{\Delta E_{in}^{(1)}}{2} \quad . \qquad (4.32)$$

Several iterations may be required if the energy loss in the film is an appreciable fraction of E_0. The final $(Nt)_i^{(f)}$ values are calculated using Eq. (4.3) with $E = \overline{E}^{(f)}$, where $\overline{E}^{(f)}$ is the final mean energy obtained from the iteration process. If the scattering is Rutherford and the film is not too thick

$$(Nt)_i^{(f)} = \left(\frac{\overline{E}^{(f)}}{E_0}\right)^2 (Nt)_i^{SEA} \quad . \tag{4.33}$$

4.3 SAMPLE ANALYSIS

This section starts with a very brief description of apparatus and operating conditions in a "typical" backscattering laboratory. The specific laboratory which is described was chosen for reasons of familiarity and concreteness. Procedures for determining certain necessary experimental quantities such as analysis beam energy, pulse-height-analyzer energy/channel, etc., are also briefly described. Examples of actual data analysis follow. Several of these analyses are explicitly done "by hand" to clearly illustrate the power and simplicity of the technique. The section concludes with a brief discussion of computer-assisted data analysis, which is, of course, currently used for most analyses.

Most of the data for the sample analyses described in this section were acquired with the standard backscattering setup described in Leavitt (1987). Ion beams from a vertical single-ended 5.5 MV Van de Graaff were deflected through 90° by a bending magnet into a horizontal collimating beam-line that preceded the target chamber. A 25 mm² surface barrier detector, placed about 150 mm upstream from the target holder at an angle 10° below the beam (Cornell geometry), subtended solid angle $\Omega = 0.78$ msr at the target. Hence, the backscattering angle, $\theta = 170°$. Detector pulses due to the backscattered analysis ions were preamplified, shaped and amplified, and sorted by a pulse-height-analyzer (PHA). The result, in the form of counts/channel vs. channel number, constituted the backscattering spectrum of the target. These data were sent to a PC for disk storage, integration of peaks, plotting, data analysis, etc. Some typical operating conditions and parameter ranges for this system are given in Table 4.1.

The beam energy (or the bending-magnet field) was calibrated using three (α,γ) resonances in ^{24}Mg (Endt and van der Leun, 1967), and (α,α) resonances in ^{14}N (Herring, 1958) and ^{16}O (Häusser et al., 1972), which covered the ^{4}He beam-energy range 2437.4 keV to 5058 keV. See

Table 4.1. Typical experimental operating conditions and parameter ranges used during acquisition of backscattering spectra described in Section 4.3.

Experimental parameter	Units	Values
Analysis ion energy	MeV	1.0-5.0
Beam cross section	mm × mm	1.5 × 1.5
Beam current	nA	10-200
Integrated charge	μC	5-100
Detector energy resolution for ^{4}He ions	keV	15
Data acquisition time	min	5-10
Vacuum	Torr	2×10^{-6}
Pump-down time	min	15

Appendix 17 for additional calibration points. The beam energy was known to ± 5 keV and was stable to less than 1 keV; the beam-energy spread was less than 0.5 keV.

The conversion of PHA channel number, n, to backscattered ion energy, E_1, was accomplished by least-squares fitting

$$E_1 = n\, \mathcal{E} + E' \tag{4.34}$$

to backscattering peak data (n_i, E_1^i) from a very thin film containing Ta, Nb, Al, and O on a C substrate. The value of E_1^i for the ith film element was calculated with Eq. (4.1) using known values of K_i and E_0. The value of n_i, the peak channel for the ith element was read from the spectrum (see Appendix C in Chu et al., 1978). Thus, values of energy/channel, $\mathcal{E}$, and energy intercept, E', were determined for the amplifier gain used.

The number of analysis ions, Q, incident on the target was calculated from the total charge, Q', deposited in the insulated target chamber during the run; $Q = Q'/e$, where $e = 1.602 \times 10^{-19}$ Coulombs. It was assumed that the incident ions bore charge +e. (See Chapter 12 for possible corrections.) The charge Q' was divided by the dead-time correction factor, DTR, to account for the fact that the PHA did not accept pulses during a portion of the time while Q' was being collected. The DTR factor was usually taken as the ratio of the "real" time to "live" time (both supplied by the PHA); this factor was usually $\lesssim 1.02$ for the analyses discussed below. Other methods for determining the DTR factor are discussed in Chapter 12.

Daily measurement of the areal density of a secondary standard Ta film, which had been calibrated with a Bi-implanted-in-Si RBS standard (Eshbach, 1983), provided

another correction factor C_{Bi}. This factor was related to the efficiency of charge collection and the value of solid angle used. Its value was that required to give the correct areal density for the Ta standard. Typical C_{Bi} values were near 1.00 with an uncertainty of ± 0.03; this uncertainty of ~ 3% included the uncertainties in charge collection and solid angle measurement as well as the uncertainty (2.5%) in the Bi RBS standard itself.

A number of apparatus parameters and measured or calculated quantities were usually considered known prior to acquisition of data for a particular sample; a summary of these is given in Table 4.2. Certain other quantities peculiar to a particular run on a particular sample are listed in Table 4.3.

4.3.1 Thin film analysis

4.3.1.1 The peak integration method

If the backscattering peaks are well separated so the integrated peak counts, A_i, can be accurately determined from the spectrum, then the *peak integration* method may be applied in the simple direct manner discussed in Section 4.1. A slightly modified version of Eq. (4.3)

$$(Nt)_i = \frac{A_i \cos\theta_1 \cdot DTR \cdot C_{Bi} \cdot e}{Q' \cdot \Omega \cdot \sigma_R^i (E, \theta) \cdot \left(\dfrac{\sigma}{\sigma_R}\right)_i} \qquad (4.35)$$

should be used for the calculation of $(Nt)_i$, the areal density of the ith element in the film. The symbols are defined in Tables 4.2 and 4.3. The ratio, $(\sigma/\sigma_R)_i$, is the non-Rutherford correction factor discussed in 4.2.2.3. Note that in instances where the integrated charge and solid angle are not well known, the quantity $C_{Bi}/(Q'\cdot\Omega)$ may be obtained from the substrate (if there is one), assuming the stopping cross section factor and scattering cross section is known for the substrate.

The spectrum shown in Fig. 4.1 is actually that of a Gd Fe film on a Si substrate; the analysis beam ions were 3776 keV ^{4}He. Example 4.4 uses data taken from this spectrum to provide element identification, elemental areal densities, the stochiometric ratio, and a "thickness" estimate for this film.

Table 4.2. Quantities whose values are usually known prior to acquisition of backscattering data for a particular sample.

Symbol	Quantity
M_1, Z_1	Identity (mass and atomic number) of the analysis ions
E_0	Incident laboratory kinetic energy of the analysis beam ions
θ	Laboratory angle through which the analysis ion is scattered
Ω	Solid angle subtended by the detector at the target
θ_1, θ_2	Angles between the sample normal and the incident and backscattered beams, respectively
$\mathcal{E}, E'$	Energy/channel and energy intercept, respectively; parameters connecting the backscattered energy, E_1, of an analysis ion with the PHA channel number, n, by $E_1 = n\mathcal{E} + E'$
C_{Bi}	Correction factor (related to efficiency of charge collection and solid angle measurement) that gives correct $(Nt)_{Bi}$ for Bi RBS standard
$K_i(\theta)$	The kinematic factor for target element i and backscattering angle θ
$\sigma_i(E,\theta)$	Cross sections for scattering of analysis ions of laboratory energy, E, through angle θ, for the ith target element
$\varepsilon^i(E)$	Stopping cross sections for analysis ions of laboratory energy E in the ith target element

Table 4.3. Quantities whose values are determined by a particular run on a particular sample.

Symbol	Quantity
Q'	Integrated charge deposited on the sample during the run
DTR	Dead-time-ratio for the PHA during the run
n_i	Channel number (at half-maximum) of the high-energy edge of the signal due to scattering from the ith target element at the sample surface
n_i'	Channel number (at half-maximum) of the low-energy edge of the backscattering peak due to the ith target element
$H_{i,0}$	Spectrum height (counts/channel) of the signal due to scattering from the ith target element at the sample surface
A_i	Integrated counts in the peak due to scattering from the ith element (in a thin film)
ΔE_i	Energy width of the peak due to scattering from the ith target element (in a thin film)

EXAMPLE 4.4. This example is an application of the peak integration method to analysis of the two-element thin film whose spectrum is shown in Fig. 4.1.

- *A priori* acquisition parameters (the symbols are defined in Table 4.2).

$E_0 = 3776$ keV $\theta = 170°$

$\theta_1 = 0°$ $\theta_2 = 10°$

$\Omega = 0.78$ msr $C_{Bi} = (0.99 \pm 0.03)$

$\mathcal{E} = (3.742 \pm .005)$ keV/ch $E' = (8 \pm 3)$ keV

$K_{Fe}(170°) = 0.7520$ $K_{Gd}(170°) = 0.9039$
                                     (from Appendix 5)

$$\sigma_R^{Fe}(E_0, 170°) = \frac{3.521}{(3.776)^2} \times 10^{-24}$$

$$= 0.2469 \times 10^{-24} \frac{cm^2}{sr}$$

$$\sigma_R^{Gd}(E_0, 170°) = \frac{21.53}{(3.776)^2} \times 10^{-24}$$

$$= 1.510 \times 10^{-24} \frac{cm^2}{sr}$$

(from Appendix 6)

$$\left(\frac{\sigma}{\sigma_R}\right)_{Fe} = 1 - \frac{(0.049)(2)(26)^{4/3}}{3776} = 0.998$$

$$\left(\frac{\sigma}{\sigma_R}\right)_{Gd} = 1 - \frac{(0.049)(2)(64)^{4/3}}{3776} = 0.993$$

[from Eq. (4.12)]

$\varepsilon^{Fe}(3776$ keV$) = 51.4 \times 10^{-15}$ eV cm^2

$\varepsilon^{Fe}(3676$ keV$) = 52.2 \times 10^{-15}$ eV cm^2

$\varepsilon^{Gd}(3776$ keV$) = 86.3 \times 10^{-15}$ eV cm^2

$\varepsilon^{Gd}(3676$ keV$) = 87.5 \times 10^{-15}$ eV cm^2

(from Appendix 3)

- Parameter values directly associated with the spectrum shown in Fig. 4.1 (the symbols are defined in Table 4.3).

$$Q' = 20.01 \ \mu C \ ; DTR = 1.008 \ ;$$
$$n_B = (757 \pm 1) \ ; n_A = (910 \pm 1)$$
$$n_B' = (660 \pm 1), n_A' = (812 \pm 1)$$
$$H_{A,0}^{AB} = (1020 \pm 20) \ cts; \ H_{B,0}^{AB} = (640 \pm 20) \ cts$$

Integrated counts in spectral regions of interest (initial and final channel numbers are listed):

channels (789 – 918) = 103978 cts ; (920 – 960) = 49 cts

channels (640 – 767) = 64957 cts ; (768 – 788) = 79 cts

- Element identification [using Eqs. (4.34) and (4.1)].

$E_1^B = n_B \mathcal{E} + E' = (757 \pm 1)(3.742 \pm 0.005) + (8 \pm 3)$
$\quad = (2841 \pm 6)$ keV

$E_1^A = n_A \mathcal{E} + E' = (910 \pm 1)(3.742 \pm 0.005) + (8 \pm 3)$
$\quad = (3413 \pm 7)$ keV

$$K_B = \frac{E_1^B}{E_0} = \frac{(2841 \pm 6)}{(3776 \pm 5)} = 0.752 \pm 0.002$$

$$K_A = \frac{E_1^A}{E_0} = \frac{(3413 \pm 7)}{(3776 \pm 5)} = 0.904 \pm 0.002$$

Therefore, elements A and B are Gd and Fe, respectively. (Note that element A could also be Tb, since $K_{Tb} = 0.9048$.)

- Calculation of elemental areal densities, $(Nt)_i$.

First, the A_i are calculated from the integrated counts in the regions of interest. In this instance, a constant background, determined by the counts/ch just above the particular peak, is subtracted.

$$A_{Fe} = 64957 - \frac{79}{21}(128) = (64475 \pm 261) \ cts$$

$$A_{Gd} = 103978 - \frac{49}{41}(130) = (103823 \pm 323) \ cts$$

In this case, the background correction is almost negligible; the calculated uncertainties in the A_i are statistical.

Next, the areal densities in the surface energy approximation, $(Nt)_i^{SEA}$, are calculated using Eq. (4.35) with $E = E_0$

$$(Nt)_{Fe}^{SEA} = \frac{(64475 \pm 261)(1.008)(0.99 \pm 0.03)(1.602 \times 10^{-19})}{(20.01 \times 10^{-6})(0.78 \times 10^{-3})(0.2469 \times 10^{-24})(0.998)} \text{ atoms/cm}^2$$

$$= (2.68 \pm 0.08) \times 10^{18} \text{ atoms/cm}^2$$

$$(Nt)_{Gd}^{SEA} = (0.709 \pm 0.021) \times 10^{18} \text{ atoms/cm}^2 \quad .$$

Then the mean energy of the ^{4}He ion in the film, $\overline{E}^{(1)}$ is calculated (in first order) using Eq. (4.29) for the first-order energy loss, ΔE_{in}^{SEA}, of the ions in the film and Eq. (4.30)

$$\Delta E_{in}^{SEA} = \epsilon^{Fe}(E_0)(Nt)_{Fe}^{SEA} + \epsilon^{Gd}(E_0)(Nt)_{Gd}^{SEA}$$

$$= (51.4 \times 10^{-15})(2.68 \times 10^{18})$$

$$+ (86.3 \times 10^{-15})(0.709 \times 10^{18}) \text{ eV}$$

$$= 199 \text{ keV}$$

$$\overline{E}^{(1)} = E_0 - \frac{\Delta E_{in}^{SEA}}{2} = 3776 - \frac{199}{2} = 3676 \text{ keV} \quad .$$

The areal densities, $(Nt)_i^{(1)}$, including the first-order correction for energy loss in the film are [adjusting the Rutherford cross section in Eq. (4.35) to the mean energy in the sample, using the inverse square dependence on energy]

$$(Nt)_{Fe}^{(1)} = \left(\frac{3676}{3776}\right)^2 (Nt)_{Fe}^{SEA} = 2.54 \times 10^{18} \text{ atoms/cm}^2$$

$$(Nt)_{Gd}^{(1)} = 0.672 \times 10^{18} \text{ atoms/cm}^2 \quad .$$

Results of an additional iteration of this procedure using Eqs. (4.31), (4.32), and (4.33) (note that ϵ^{Fe} and ϵ^{Gd} are evaluated at $\overline{E}^{(1)}$) are

$$\Delta E_{in}^{(1)} = (52.2 \times 10^{-15})(2.54 \times 10^{18})$$

$$+ (87.5 \times 10^{-15})(0.672 \times 10^{18}) \text{ eV}$$

$$= 191 \text{ keV}$$

$$\overline{E}^{(2)} = 3776 - \frac{191}{2} = 3681 \text{ keV}$$

$$(Nt)_{Fe}^{(2)} = \left(\frac{3681}{3776}\right)^2 (Nt)_{Fe}^{SEA}$$

$$= (2.55 \pm 0.08) \times 10^{18} \text{ atoms/cm}^2$$

$$(Nt)_{Gd}^{(2)} = (0.674 \pm 0.021) \times 10^{18} \text{ atoms/cm}^2 \quad .$$

Additional iterations produce no further change in the $(Nt)_i$ values, so these are the final values of energy loss in the film, mean analysis ion energy in the film, as well as the elemental areal densities given by the mean energy approximation.

• The average stoichiometric ratio for this film may be calculated using Eq. (4.5)

$$\frac{N_{Fe}}{N_{Gd}} = \frac{A_{Fe}}{A_{Gd}} \cdot \frac{\sigma_R^{Gd}(E_0, 170°)}{\sigma_R^{Fe}(E_0, 170°)} \cdot \frac{\left(\dfrac{\sigma}{\sigma_R}\right)_{Gd}}{\left(\dfrac{\sigma}{\sigma_R}\right)_{Fe}}$$

$$= \frac{(64475 \pm 261)}{(103823 \pm 323)} \cdot \frac{21.53}{3.521} \cdot \frac{0.993}{0.998}$$

$$= 3.78 \pm 0.02 \quad .$$

If the "molecular" formula for the film is written $Gd_m Fe_n$, then $m = 0.209 \pm 0.001$, $n = 0.791 \pm 0.001$. The quoted uncertainties are statistical, that is, due to the uncertainty in the A_i ratio. The cross section ratio has been regarded as exact in this calculation. The cross sections for He-Fe and He-Gd, except for the small electron shell corrections, are believed to be Rutherford at the analysis energy used. Of course, an assigned cross section ratio uncertainty may be easily included in the calculation (see Chapter 11).

• The *value* of the physical film thickness, t, could be calculated using Eqs. (4.6) and (4.7) if the density of the film were known. It was not, in this instance. However, it is customary to produce an *estimate* of the film thickness in such cases using the following procedure. The actual Gd Fe mixture is replaced by an elemental bilayer with the same areal densities for Gd and Fe. The elemental layers are assumed to have elemental bulk densities. The thickness of this replacement film serves as the *estimate* of the physical thickness of the original film. The values of elemental

bulk densities $N_{Fe} = 8.44 \times 10^{22}$ atoms/cm^3, $N_{Gd} = 3.02 \times 10^{22}$ atoms/cm^3 are obtained from Appendix 1. Hence, from Eq. (4.7)

$$t_{Fe} = \frac{2.55 \times 10^{18}}{8.44 \times 10^{22}} \text{ cm} = 302 \text{ nm}$$

$$t_{Gd} = \frac{0.674 \times 10^{18}}{3.02 \times 10^{22}} \text{ cm} = 223 \text{ nm}$$

$$t_{GdFe} \sim 525 \text{ nm} .$$

Note that no uncertainty is assigned to this final thickness estimate. In addition, the judicious analyst should indicate that this *estimate* may not accurately represent the actual physical thickness of the film.

• Summary of the analysis results for the two-element film of Fig. 4.1. The stoichiometric ratio is

$$\frac{N_{Fe}}{N_{Gd}} = 3.78 \pm 0.02$$

so the stoichiometry of the film is $Gd_{(0.209 \pm 0.001)}$ $Fe_{(0.791 \pm 0.001)}$. The areal densities are

$$(Nt)_{Fe} = (2.55 \pm 0.08) \times 10^{18} \text{ atoms/cm}^2$$

$$(Nt)_{Gd} = (0.674 \pm 0.021) \times 10^{18} \text{ atoms/cm}^2 .$$

The film thickness is about 0.5 μm. Note that the uncertainty in the ratio N_{Fe}/N_{Gd} is about 0.5%, while the $(Nt)_i$ values are uncertain by about 3%. This is a typical result and reflects the cancellation of the hard-to-measure quantities Q and Ω from the ratio.

The peak integration method may be applied in this simple and direct manner to the analysis of any single-layer film whose backscattering peaks do not overlap. It is not necessary that film composition be uniform as a function of depth. The resulting stoichiometric ratios will, of course, be the *average* values for the film. For very thin films, the backscattering peaks will not have the nearly flat portions on top but will be sharp peaks; in this instance, the channel numbers of the peak *centers* should be used in Eqs. (4.1) and (4.34) for element identification (see Appendix C in Chu *et al.*, 1978).

Multilayer films

The peak integration method may also be applied to the analysis of multilayer films. The spectrum of a trilayer film on a C substrate is shown in Fig. 4.4. The peaks associated with a particular layer may be identified by noting peak locations in spectra taken at different tilt angles (θ_1). The high-energy edges of the peaks associated with the surface layer have the same locations in these spectra. Buried-layer peak locations shift toward lower energies as the tilt angle is increased since the effective overlayer thicknesses increase with tilt angle as $(\cos \theta_1)^{-1}$. The locations of peaks associated with a particular buried layer all shift by about the same number of channels as the tilt angle is varied. Two backscattering spectra, one taken with $\theta_1 \sim 0°$ and the other with θ_1 between 45° and 60°, are usually sufficient for assignment of the peaks to appropriate layers. Once the peaks have been assigned to layers, the peak integration method may be applied to successive layers, starting with the surface layer.

The analysis ion energy incident on a particular layer is, of course, the energy E_0 minus the energy lost by the ions traversing the layers that cover the layer being analyzed. The $(Nt)_i$ for a particular layer should be calculated in the mean energy approximation before proceeding to the next layer. In the case of the spectrum shown in Fig. 4.4, the peak integration method may be only partially applied. The stoichiometry and areal densities of the $Al_2O_3(Ar)$ layers may be completely determined. But the NiFe layer stoichiometry cannot be determined from these data since the Ni and Fe peaks overlap. For this spectrum, the Ni and Fe edges are separated by less than 10 channels. The surface barrier detector energy resolution ($\delta E \doteq 15$ keV) is about 8 channels, and in addition, both Fe and Ni have several isotopes. The result is that this particular NiFe film is probably too thick for accurate determination of its stoichiometry by ^{4}He ion beam analysis with surface barrier detectors. Films of NiFe as thick as 25nm may be analyzed with 5 MeV ^{4}He (Leavitt *et al.*, 1985). In such cases, thinner "witness" films, made by the same deposition procedures, are sometimes used to provide the stoichiometric